Blood Glucose Prediction Using Stochastic Modeling in Neonatal Intensive Care

Aaron J. Le Compte*, Dominic S. Lee, J. Geoffrey Chase, Jessica Lin, Adrienne Lynn, and Geoffrey M. Shaw

***Abstract*—Hyperglycemia is a common metabolic problem in premature, low-birth-weight infants. Blood glucose homeostasis in this group is often disturbed by immaturity of endogenous regulatory systems and the stress of their condition in intensive care. A dynamic model capturing the fundamental dynamics of the glucose regulatory system provides a measure of insulin sensitivity (S_I). Forecasting the most probable future S_I can significantly enhance real-time glucose control by providing a clinically validated/proven level of confidence on the outcome of an intervention, and thus, increased safety against hypoglycemia. A 2-D kernel model of S_I is fitted to 3567 h of identified, time-varying S_I from retrospective clinical data of 25 neonatal patients with birth gestational age 23 to 28.9 weeks. Conditional probability estimates are used to determine S_I probability intervals. A lag-2 stochastic model and adjustments of the variance estimator are used to explore the bias-variance tradeoff in the hour-to-hour variation of S_I. The model captured 62.6% and 93.4% of in-sample S_I predictions within the (25th–75th) and (5th–95th) probability forecast intervals. This overconservative result is also present on the cross-validation cohorts and in the lag-2 model. Adjustments to the variance estimator found a reduction to 10%–50% of the original value provided optimal coverage with 54.7% and 90.9% in the (25th–75th) and (5th–95th) intervals. A stochastic model of S_I provided conservative forecasts, which can add a layer of safety to real-time control. Adjusting the variance estimator provides a more accurate, cohort-specific stochastic model of S_I dynamics in the neonate.**

***Index Terms*—Forecasting, human factors, stochastic approximation.**

I. Introduction

HYPERGLYCEMIA occurs in 40%–80% of very low-birth-weight infants in the neonatal intensive care unit (NICU) [3], [4]. Low-birth-weight neonates and preterm neonates are at the highest risk of developing hyperglycemia [5], [6], even in patients with no family history of diabetes. Hyperglycemic infants are often treated by glucose restriction [11]–[13]. However, prolonged severe glucose restriction may adversely affect the infant's nutritional status, and may also be a reason for poor growth observed in these infants [11]. Avoiding hyperglycemia, while providing adequate nutrition to promote growth and development, is a major challenge for healthcare providers in the NICU.

Several mechanisms are thought to contribute to neonatal hyperglycemia. Persistent endogenous glucose production (EGP) during glucose infusions has been demonstrated in several studies [9], [16]. Hyperglycemia is also common during times of neonatal stress and increased secretion of counter-regulatory hormones leads to a prominent rise in endogenously produced glucose, as well as a reduction in insulin sensitivity (S_I). Nutritional support regimes with high carbohydrate content are also provided to increase neonate weight, but often compound the counter-regulatory response [17]. Immaturity of the glucose transport system and a limited number of insulin-dependent tissues are also thought to be contributing factors [18].

Insulin is an anabolic hormone and promotes growth, while lowering glucose levels. However, endogenous deficiency or lack of effect due to high insulin resistance will have a negative impact on glycaemic levels [11]. Immature insulin processing in the neonate produces excessive proinsulin, which is approximately 16× less effective than regular adult insulin, which may also explain why some poor control is exhibited in this population [21]. Preterm infants require higher insulin concentrations that term infants to maintain euglycemia [21], and a high insulin concentration compared to adults may be required to promote peripheral glucose uptake [9]. Besides glucose control, reduced proteolysis, and thus, preservation of muscle mass has been associated with insulin therapy in this cohort [7], [8], independent of glucose infusion [26].

Several recent studies have associated hyperglycemia with increased morbidity and mortality in neonatal cohorts [27]–[29]. Limited trials of glucose control using insulin in neonates have been reported [7], [11], [34]–[39], and insulin therapy did help to improve glucose tolerance in these limited trials. Insulin therapy in preterm neonates is gaining wider acceptance [40], [41], but still carries the risk of hypoglycemia and possible neurological complications [3].

Model-based glycaemic control methods using both insulin and/or nutrition modulation have been employed successfully in the control of hyperglycemia in adult critical care populations, as reviewed by Chase *et al.* [42]. Model-based methods allow information about the fundamental metabolic state of the patient, S_I in this case, to be inferred from serial blood

Manuscript received June 7, 2009; revised September 21, 2009. First published October 30, 2009; current version published February 17, 2010. This work was supported in part by the New Zealand Tertiary Education Commission. *Asterisk indicates corresponding author.*

*A. J. Le Compte is with the Department of Mechanical Engineering, University of Canterbury, Christchurch 8041, New Zealand (e-mail: ajc190@student.canterbury.ac.nz).

D. S. Lee is with the Department of Mathematics and Statistics, University of Canterbury, Christchurch 8140, New Zealand.

J. G. Chase and J. Lin are with the Department of Mechanical Engineering, University of Canterbury, Christchurch 8041, New Zealand (e-mail: geoff.chase@canterbury.ac.nz).

A. Lynn is with the Neonatal Department, Christchurch Women's Hospital, Christchurch 4711, New Zealand.

G. M. Shaw is with the Department of Intensive Care, Christchurch Hospital, Christchurch 4710, New Zealand.

Color versions of one or more of the figures in this paper are available online at http://ieeexplore.ieee.org.

Digital Object Identifier 10.1109/TBME.2009.2035517

glucose (BG) measurements, and records of nutrition and insulin administration [2], [43]. Once the current S_I of the infant has been identified, prediction of future S_I would allow predictions of outcome BG concentration for an intended clinical intervention. Changes in the S_I parameter reflect variations in patient condition such as clinical stress [44], [45] and drug therapy [13]. Thus, tracking and forecasting this parameter is important to provide safe glycaemic control in the highly dynamic preterm neonate.

Stochastic models provide a means to quantify this probability of a future S_I [46]. Thus, the resulting distribution of BG concentrations that would result from a given intervention can be determined [47]. This information can then be used to guide dosing to avoid low blood sugar concentrations, improve overall glycaemic control, and identify periods of potential high glucose variability that may be indicative of emerging clinical events.

This paper presents the adaptation of a stochastic model for S_I prediction from adult critical care to the unique clinical and physiological case of the neonate. Several modifications to the initial kernel density estimation model are used to explore the relationship between the model and the underlying dataset. In addition, the stochastic modeling approach is extended to include more than the prior hour values to determine if improved prediction can be obtained in this neonatal case.

II. Methods

A. Patient Cohort

Retrospective data from 25 episodes of insulin therapy treatment in Christchurch Women's NICU were used in the study. Ethics approval for the collection and publication of data was obtained from the Upper South Regional Ethics Committee. The 25 episodes of insulin usage were composed of 21 individual patients representing 3567 h of patient data. Gestational age at birth ranged from 23 to 28.9 weeks, and birth weight ranged from 600 to 1280 g. Inclusion criteria were birth weight less than 1500 g and a period of treatment with insulin of at least 12 h.

B. System Model

The system model used in this research is based on a clinically validated glucose regulatory system model for adult intensive care patients [2], [43]. The model has been modified to better account for the main physiological differences in neonates based on available clinical data and kinetic studies. The overall model is defined as

$$\dot{G} = -p_G G - S_I G \frac{Q}{1+\alpha_G Q} + \frac{P(t) + (P_{\mathrm{END}} m_{\mathrm{body}}) - (\mathrm{CNS} m_{\mathrm{brain}})}{(V_{G,\mathrm{frac}}(t) m_{\mathrm{body}})} \quad (1)$$

$$\dot{Q} = -kQ + kI \quad (2)$$

$$\dot{I} = -\frac{nI}{1+\alpha_I I} + \frac{u_{\mathrm{ex}}(t)}{(V_{I,\mathrm{frac}} m_{\mathrm{body}})} + e^{-(k_I u_{\mathrm{ex}}(t))} I_B \quad (3)$$

TABLE I
Constant Model Parameter Values

Parameter	Value	References
k	0.0086 min^{-1}	[2]
n	0.90 min^{-1}	[7-10]
α_I	1.70 x 10^{-3} L/mU	[2]
α_G	0 L/mU	[9]
CNS	0.088 mmol/kg/min	[14]
m_{brain}	0.14 * m_{body} kg	[15]
I_B	10 mU/L/min	[9, 10]
$V_{I,frac}$	0.045 L/kg	[19, 20]
$V_{G,frac}$	ECF proportion[a] L/kg	[22-25]
P_{END}	0.02838 mmol/kg/min	[1, 10, 16, 26, 30-33]
p_G	0.003 min^{-1}	[1]

where $G(t)$ (in millimols per liter) is the total plasma glucose and $I(t)$ (in millimols per liter) is the plasma insulin, exogenous insulin input is represented by $u_{\mathrm{ex}}(t)$ (in milliunits per minute), and basal endogenous insulin secretion I_B [in milliunits per (liter·minute)], with k_I representing the suppression of basal insulin secretion in the presence of exogenous insulin. The effect of previously infused insulin being utilized over time is represented by $Q(t)$ (in milliunits per liter), with k [1/min] accounting for the effective life of insulin in the system. Body weight and brain weight are denoted by m_{body} (in kilograms) and m_{brain} (in kilograms), respectively. Patient endogenous glucose clearance and insulin sensitivity are p_G [1/min] and S_I [in liters per (milliunits·minutes), respectively. The parameter $V_{I,\mathrm{frac}}$ (in liters per kilogram) is the insulin distribution volume per kilogram body weight and n [1/min] is the constant first-order decay rate for insulin from plasma. Total plasma glucose input is denoted $P(t)$ (in millimols per minute), EGP is denoted by P_{END} [in millimols per (kilogram·minutes)] and $V_{G,\mathrm{frac}}$ (in liters per kilogram) represents the glucose distribution volume per kilogram of body weight. CNS [in millimols per (kilogram·minutes)] represents noninsulin-mediated glucose uptake by the central nervous system, as well as the liver, kidneys, and red blood cells [48]. Michaelis–Menten functions are used to model saturation, with α_I (in liters per milliunit) used for the saturation of plasma insulin disappearance, and α_G (in liters per milliunit) for the saturation of insulin-dependent glucose clearance.

Table I summarizes the parameters used in this model. For the simulations in this study, k, n, α_I, α_G, CNS, I_B, $V_{I,\mathrm{frac}}$, p_G, and P_{END} are set to generic population values based on reported data. Prior clinical and model sensitivity studies with the similar adult model [2], [49] have shown this choice to be robust. The glucose compartment (1) in this model was modified from [2] and [49] to account for available neonatal data [50]. In particular, the CNS and P_{END} terms were introduced to take advantage of available neonatal glucose kinetic studies. The endogenous glucose clearance term p_G was set to $0.003\ \mathrm{min}^{-1}$ based on parameter sensitivity studies [1], and is considered effectively constant, similar to the adult case [2]. Insulin-mediated glucose uptake saturation represented by the parameter α_G was set to zero based on the results of [9] and [51], which showed no saturation in glucose uptake with increasing insulin concentration

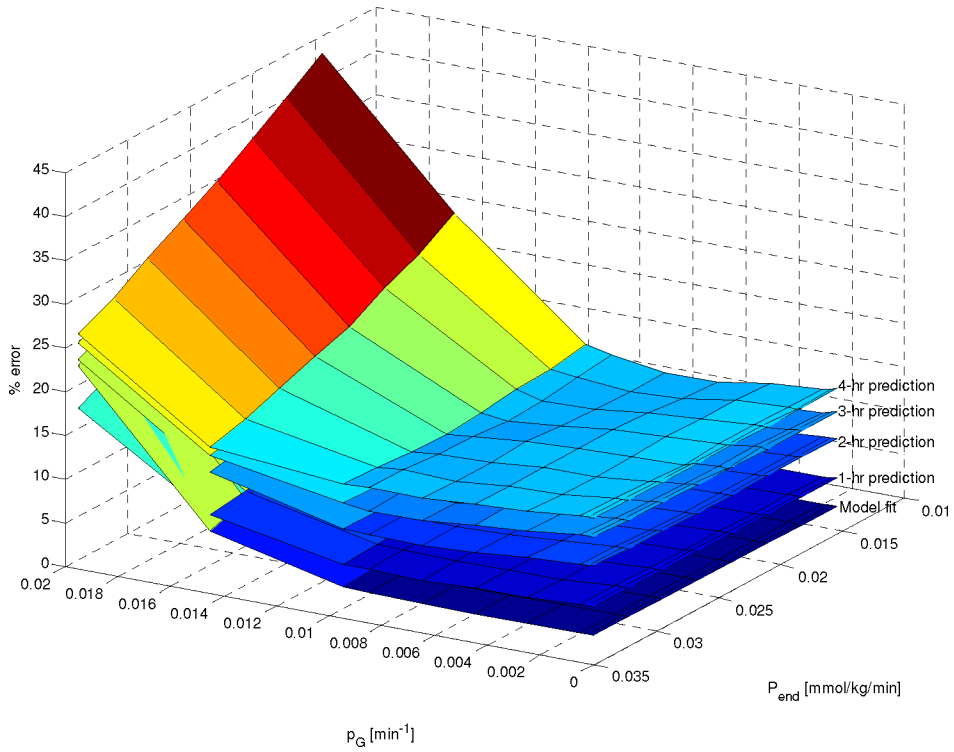

Fig. 1. Cohort percentage BG fit error and model prediction error for several values of EGP (P_{END}) and endogenous glucose clearance (p_G). Fit and prediction quality is very robust to the value of p_G and P_{END} utilized [1].

within typical clinical usage ranges. Fig. 1 shows the model fit and 1–4 h prediction error for a range of physiological p_G and P_{END} values over the 3567 h of retrospective patient data. Model fit and prediction performance metrics were robust to a range of p_G and P_{END} values. Further parameter sensitivity analysis found that model performance was robust to variations of the parameters presented in Table I [1].

The parameter S_I is explicitly determined from the data. The integral-based fitting method of Hann *et al.* [2] was employed for identifying S_I over time using retrospective BG concentrations (G), insulin administration ($u_{\mathrm{ex}}(t)$), and nutritional infusion rates ($P(t)$). The resulting time-varying S_I profile was constrained to a lower bound of 1×10^{-5} L/(mU·min) to prevent nonphysiological negative values for S_I [46], [47].

C. Stochastic Model (Lag-1)

A 2-D kernel density estimation method is used to construct the stochastic model that describes the hourly transition of S_I. The kernel density method combines probability distribution functions for each point of data to generate an overall density function for the dataset. This method has the advantage of producing a smooth, physiologically likely, continuous function across the parameter range to provide continuity when interpolating S_I forecasts to account for each particular patient state, and automatically accounts for any possible multimodality where the density of data may show several distinct peaks corresponding to patterns of changes in S_I. The overall result is a bivariate probability density function for the potential parameter values. The goal of this statistical model is to quantify the range of S_I one hour ahead in time ($S_{I,n+1}$) based on available data ($S_{I,n}, S_{I,n-1}, S_{I,n-2}, \ldots, S_{I,0}$) to guide real-time clinical control. Thus, it is important that the model formulation is computationally feasible for real-time applications on typical hardware.

The 2-D kernel density method is chosen for creating the stochastic model because the distribution of $S_{I,n+1}$ varies with $S_{I,n}$, as shown in Fig. 2, and cannot be simply described with a single standard statistical distribution. Thus, the variations in S_I can be treated as a Markov process. A Markov process has the property that the conditional probability density function of future states of the process, given the current state, depends only upon the current state. Therefore, using the Markov property of the stochastic behavior of S_I, the conditional probability density of $S_{I,n+1}$ taking on a value y can be calculated by knowing $S_{I,n} = x$

$$p\left(S_{I,n+1} = y | S_{I,n} = x\right) = \frac{p\left(S_{I,n+1} = y, S_{I,n} = x\right)}{p\left(S_{I,n} = x\right)}. \quad (4)$$

Considering the fitted S_I in a 2-D space, as shown in Fig. 2, the joint probability density function across the x–y ($S_{I,n}$–$S_{I,n+1}$) plane is defined by the fitted values shown by the dots, whose coordinates are x_i and y_i

$$p(x,y) = \frac{1}{n}\sum_{i=1}^{n} \frac{\phi\left(x; x_i, \sigma_{x_i}^2\right)}{p_{x_i}} \frac{\phi\left(y; y_i, \sigma_{y_i}^2\right)}{p_{y_i}} \quad (5)$$

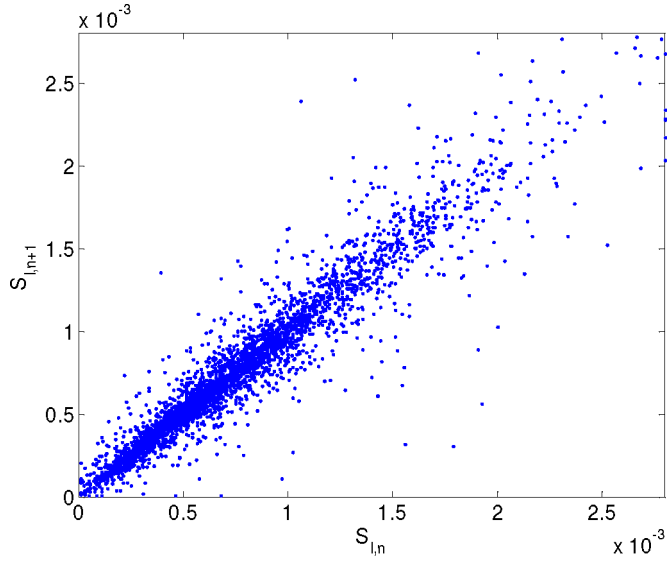

Fig. 2. Variation of fitted S_I from hour n to hour $n+1$ for 3567 h of fitted data. The distribution of $S_{I,n+1}$ changes based on the value of $S_{I,n}$ and cannot be described by a simple statistical distribution.

where

$$p_{x_i} = \int_{S_{I,\text{lower}}}^{S_{I,\text{upper}}} \phi\left(x; x_i, \sigma_{x_i}^2\right) dx \tag{6}$$

$$p_{y_i} = \int_{S_{I,\text{lower}}}^{S_{I,\text{upper}}} \phi\left(y; y_i, \sigma_{y_i}^2\right) dy. \tag{7}$$

Effectively, the joint 2-D probability density function is the normalized summation of normal probability density functions $\phi\left(x; x_i, \sigma_{x_i}^2\right)$ centered at individual data points.

In (5)–(7), the variance σ at each data point is a function of the local data density in a centered and orthonormalized space of x and y. Incorporating (6) and (7) into (5) normalizes each $\phi\left(x; x_i, \sigma_{x_i}^2\right)$ and $\phi\left(y; y_i, \sigma_{y_i}^2\right)$ in the positive domain, effectively putting boundaries along $x = S_{I,\text{lower}}$, $x = S_{I,\text{upper}}$, $y = S_{I,\text{lower}}$, and $y = S_{I,\text{upper}}$ lines, and enforcing physiological validity in S_I values. For the neonatal case, the boundary values $S_{I,\text{lower}}$ and $S_{I,\text{upper}}$ were set to 1×10^{-5} L/(mU·min) and 2.8×10^{-3} L/(mU·min), respectively, to define the computation domain based on the observed distribution of S_I found in fitting the model to the data [52].

The right-hand side denominator of (4) can be calculated by integrating (5) with respect to y. Hence, (4) can be calculated as

$$\begin{aligned} p(S_{I,n+1} = y | S_{I,n} = x) &= \frac{\sum_{i=1}^{n} \left(\phi\left(x; x_i, \sigma_{x_i}^2\right)/p_{x_i}\right)\left(\phi\left(y; y_i, \sigma_{y_i}^2\right)/p_{y_i}\right)}{\sum_{i=1}^{n} \left(\phi\left(x; x_i, \sigma_{x_i}^2\right)/p_{x_i}\right)} \\ &= \sum_{i=1}^{n} w_i(x) \frac{\phi\left(y; y_i, \sigma_{y_i}^2\right)}{p_{y_i}} \end{aligned} \tag{8}$$

where

$$w_i(x) = \frac{\left(\phi\left(x; x_i, \sigma_{x_i}^2\right)/p_{x_i}\right)}{\sum_{i=1}^{n} \left(\phi\left(x; x_i, \sigma_{x_i}^2\right)/p_{x_i}\right)}. \tag{9}$$

Thus, knowing $S_{I,n} = x$ at hour n, the probability of $S_{I,n+1} = y$ at hour $n+1$ can be calculated using (8) and (9) across the x–y plane. Where there is a higher density of data, more certainty can be drawn on the "true" behavioral pattern.

The model was cross validated by splitting the 25 patient cohort into five groups, each containing five patients. For each group, the model was fitted on the remaining 20 patients of the cohort representing approximately 2800 h of data. Out-of-sample S_I predictions were generated for the five patients of the unused group and compared to the actual fitted S_I from these five patients.

Based on the in-sample, where the stochastic model is generated from the entire retrospective dataset and tested on the same data, and out-of-sample, where different subsets of data are used for model generation and testing, the kernel density estimator was modified by multiplying the variance estimators by a constant c (i.e., $c\sigma_x$ and $c\sigma_y$) to explore the model bias-variance tradeoff for this data. This adjustment to the variance estimator effectively adjusts the kernel bandwidth and the degree of smoothing over the data.

D. Stochastic Model (Lag-2)

The stochastic model was extended to incorporate lag-2 effects to investigate any further reliance on S_I time-history to provide justification for more complex Markov-like models. The lag-2 model produces probability intervals for $S_{I,n+1} = z$ at hour $n+1$, given the S_I for the previous two hours: $S_{I,n-1} = x$ and $S_{I,n} = y$. The derivation of the model is similar to that of the lag-1 case in that the extension to 3-D data involves the product of three univariate probability distributions. Further details on higher dimensional kernel density smoothing methods are available in [53]. The resulting conditional probability estimator is defined as shown in (10) at the bottom of the next page, where

$$w_i(x, y) = \frac{\left(\phi\left(x; x_i, \sigma_{x_i}^2\right)/p_{x_i}\right)\left(\phi\left(y; y_i, \sigma_{y_i}^2\right)/p_{y_i}\right)}{\sum_{i=1}^{n} \left(\phi\left(x; x_i, \sigma_{x_i}^2\right)/p_{x_i}\right)\left(\phi\left(y; y_i, \sigma_{y_i}^2\right)/p_{y_i}\right)} \tag{11}$$

$$p_{z_i} = \int_{S_{I,\text{lower}}}^{S_{I,\text{upper}}} \phi\left(z; z_i, \sigma_{z_i}^2\right) dz. \tag{12}$$

Greater details of the general modeling approach, theoretical background, and specific computations are given in [46] and [47].

III. Results

Fig. 2 shows the distribution of hourly variation in S_I for the 3567 h of patient data. Approximately 95% of the values are below 1.5×10^{-3} L/(mU·min). Fig. 3 shows the conditional probability plot for the lag-1 model. Fig. 4 shows the 5th, 25th, 50th, 75th, and 95th percentile probability bounds computed by integrating Fig. 3, overlaid on the raw data of Fig. 2. For a given value $S_{I,n}$, the 25th–75th percentile prediction bound for $S_{I,n+1}$ is found by determining the intersection of the 25th percentile bound and the 75th percentile bound on Fig. 4 with the line $y = S_{I,n}$, shown in Fig. 4 for $S_{I,n} = 1 \times 10^{-3}$ L/(mU·min). These values can then be sequentially substituted

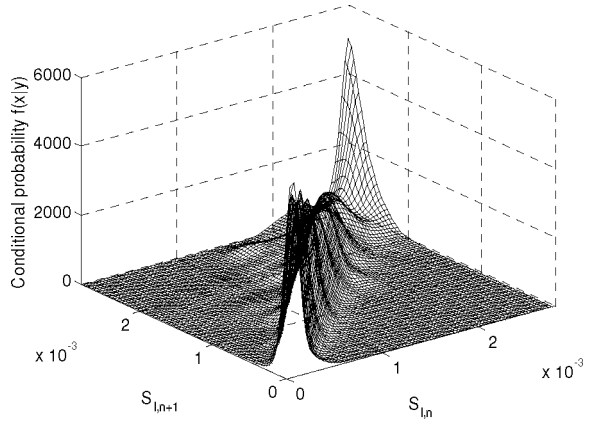

Fig. 3. Conditional probability density function for $S_{I,n+1}$ knowing $S_{I,n}$. The structure of the plot is largely unimodal in the region $S_{I,n} < 1.5 \times 10^{-3}$ and $S_{I,n+1} < 1.5 \times 10^{-3}$, corresponding to the region of densest data.

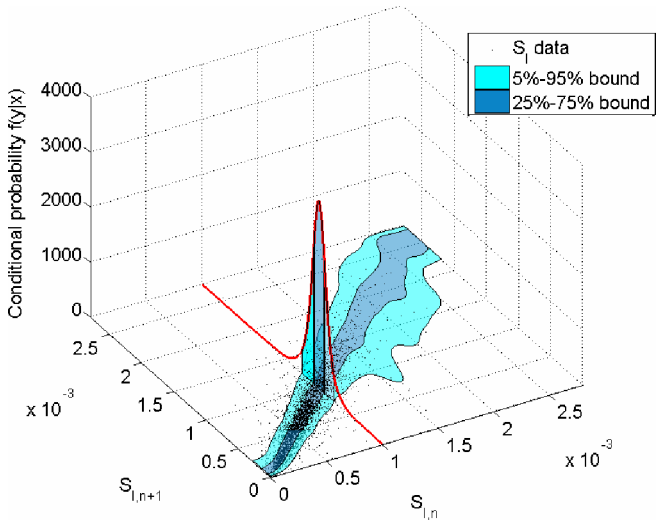

Fig. 4. Hourly S_I variation data with probability bounds. The bounds are computed using an equal-tailed method approximation. An example curve showing the computation of probability bounds for $S_{I,n} = 1 \times 10^{-3}$ L/(mU·min) is displayed.

for S_I into (1) to produce BG concentration forecasts based on an equal-tailed calculated 25th–75th percentile range of likely future S_I [47].

Table II shows the in-sample results for the lag-1 model for $n = 3530$ predictions. The number of predictions is less than the total hours of S_I due to end effects where the patient data record was not evenly divisible by 1 h, and because predictions can only be computed after the second hour of patient data. The

TABLE II
IN-SAMPLE RESULTS FOR STOCHASTIC MODEL PREDICTION WIDTHS

% S_I within prediction interval	[25th - 75th]	62.6%
	[5th - 95th]	93.4%
% BG within prediction interval	[25th -75th]	59.1%
	[5th - 95th]	92.2%
BG prediction interval width	[25th - 75th]	0.78 mmol/L
	[5th - 95th]	2.32 mmol/L
Median absolute percent BG point prediction error		4.3%
Median absolute BG point prediction error		0.34 mmol/L

Data are expressed as cohort medians ($n = 3530$ predictions).

overall median 1-h absolute prediction error comparing predicted BG based on the 50th percentile of predicted S_I to the interpolated value from retrospective data is 4.3%, corresponding to an average BG error of 0.34 mmol/L. The width of the (25th–75th) BG probability interval is 0.78 mmol/L. Similarly, the (5th–95th) BG probability interval width is 2.32 mmol/L. S_I predictions (62.6%) were within the (25th–75th) probability intervals, corresponding to 59.1% of BG predictions. Similarly, 93.4% of S_I predictions were within the (5th–95th) probability intervals, corresponding to 92.2% of BG predictions. Thus, the proportion of fitted S_I and predicted BG values that fell within the (25th–75th) and (5th–95th) probability intervals were measurably higher than the expected 50% and 90%.

Table III shows the results of the model out-of-sample cross validation. The results are generally consistent between groups, suggesting that the overall model contains sufficient data to account for the range of dynamics observed in this cohort. Table III shows that the model consistently overestimates the probability bounds, with the proportion of S_I within the bounds higher than expected for the specified bandwidth.

The results of Tables II and III suggest that the model prediction coverage for S_I is overconservative by approximately 7%–12% for the (25th–75th) prediction interval. The lag-2 model was used to investigate whether these effects could be mitigated by incorporating S_I information from two previous hours. A comparison of the lag-1 and lag-2 models revealed 61.3% of S_I fell within the (25th–75th) for the lag-2 model, similar to the 62.6% result for the lag-1 case. Similarly, 94.6% of S_I fell within the lag-2 (5th–95th) interval compared to 93.4% for the lag-1 model. These results suggest that lag-2 effects play no significant major role in the evolution of S_I compared to the simpler lag-1 case.

A comparison of the lag-1 and lag-2 models revealed 61.3% of S_I fell within the (25th–75th) for the lag-2 model, similar

$$
\begin{aligned}
p(S_{I,n+1} = z | S_{I,n-1} = x, S_{I,n} = y) &= \frac{\sum_{i=1}^{n} \left(\phi\left(x; x_i, \sigma_{x_i}^2\right)/p_{x_i}\right)\left(\phi\left(y; y_i, \sigma_{y_i}^2\right)/p_{y_i}\right)\left(\phi\left(z; z_i, \sigma_{z_i}^2\right)/p_{z_i}\right)}{\sum_{i=1}^{n} \left(\phi\left(x; x_i, \sigma_{x_i}^2\right)/p_{x_i}\right)\left(\phi\left(y; y_i, \sigma_{y_i}^2\right)/p_{y_i}\right)} \\
&= \sum_{i=1}^{n} w_i\left(x, y\right) \frac{\phi\left(z; z_i, \sigma_{z_i}^2\right)}{p_{z_i}} \qquad (10)
\end{aligned}
$$

TABLE III
CROSS-VALIDATION COMPARISON STUDY FOR THE 25 PATIENT COHORT. EACH GROUP CONTAINED FIVE PATIENTS, WITH EACH MODEL GENERATED FROM APPROXIMATELY 2800 h OF DATA

Group	Groups used to create model	% S_I within interval		% BG within interval		BG interval width (mmol/L)		BG point prediction error	BG point prediction error (mmol/L)
		[25th - 75th]	[5th - 95th]	[25th -75th]	[5th - 95th]	[25th - 75th]	[5th - 95th]		
Group 1:	[-, 2, 3, 4, 5]	57.4%	92.2%	56.4%	90.9%	0.71	2.06	4.2%	0.32
Group 2:	[1, -, 3, 4, 5]	68.7%	92.1%	64.3%	91.5%	0.75	2.17	3.7%	0.28
Group 3:	[1, 2, -, 4, 5]	67.0%	94.8%	62.4%	94.0%	0.91	2.61	4.6%	0.36
Group 4:	[1, 2, 3, -, 5]	59.2%	91.8%	56.2%	90.8%	0.87	2.48	4.8%	0.41
Group 5:	[1, 2, 3, 4, -]	61.7%	95.6%	57.1%	92.7%	0.85	2.53	5.2%	0.38
Overall	[1, 2, 3, 4, 5]	62.6%	93.4%	59.1%	92.2%	0.78	2.32	4.3%	0.34

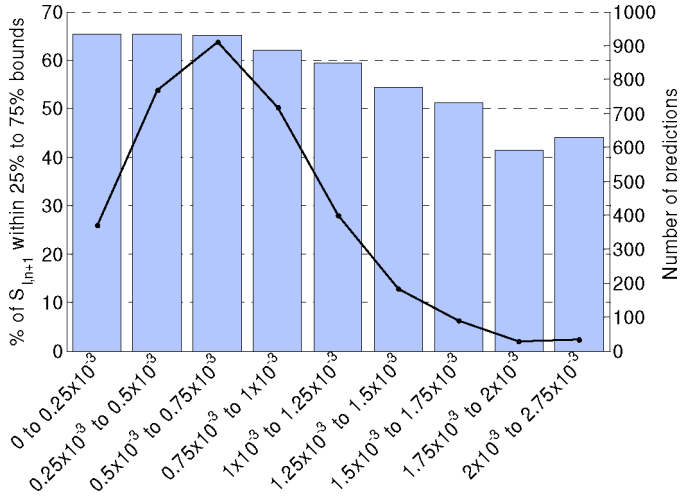

Fig. 5. Proportion of in-sample predicted S_I within the 25%–75% prediction bounds and number of predictions (=number of data points) grouped by S_I range.

to the 62.6% result for the lag-1case. Similarly, 94.6% of S_I fell within the lag-2 (5th–95th) interval compared to 93.4% for the lag-1 model. These results suggest that lag-2 effects play no significant major role in the evolution of S_I compared to the simpler lag-1 case.

Fig. 5 shows the proportion of in-sample predictions within the 25%–75% probability bound grouped by location along the $S_{I,n}$ axis. Also plotted on Fig. 5 is the number of data points (=number of in-sample predictions) for each group. The 25th–75th percentile bounds would be expected to contain approximately 50% of the data. However, Fig. 5 shows that the coverage often exceeds this expectation. This coverage discrepancy is highest where the data density is greatest. This result suggests that the local data density variance estimators (σ_x and σ_y) are conservative for this dataset.

The effect of modifying the kernel density estimation parameter is shown for several values of c in Table IV. Reductions of the variance estimators to approximately 10% – 50% (c = 0.1–0.5) of their original value yield coverage widths that contain numbers closer to the approximately expected proportion of in-sample data values.

Fig. 6 shows probability plots for $c = 1.0$, $c = 0.5$, and $c = 0.1$. As expected, the probability distribution becomes less smooth for lower values of c, particularly for higher values of S_I, where data are less dense due to the modification of the kernel bandwidth and subsequent degree of smoothing. Additionally, for lower values of c, the (25th–75th) and (5th–95th) percentile probability bounds for $S_{I,n+1}$ are essentially equal for some regions of $S_{I,n}$ due to sparse data, which may contribute to the increase in coverage proportion for c less than 0.1, and show that the model is possibly overfitting the data.

Despite the overestimation of the prediction band widths, the 50th percentile of the fitted probability distribution is centered on the data reasonably well, with 49.1% and 50.9% of in-sample predictions above and below the 50th percentile limit, respectively. Probability bounds for the $(50 - a, 50 + a)$ percentile limits can be compared to the ideal prediction coverage. Thus, for example, for $a = 10$, the proportion of predictions within the (40th and 60th) percentile limits of the model distribution can be compared to the ideal value of $(2a)\% = 20\%$.

Fig. 7 shows the extent of the model coverage overestimation across the range of prediction bounds. Thus, for the $c = 1.0$ example at $2a = 38\%$, 50% of the data lies between the 31st and 69th percentiles of the model, where the expected coverage is 38%. Similarly, 90% of the data lie between percentiles 8.5 and 92.5, where the expected coverage is a much closer 85%. The gap between actual and expected ideal bands is widest for prediction bands of 30%–60% coverage. The $c = 0.5$ case produces a line much closer to the 45° ideal.

Fig. 8 shows a simulated trial demonstrating the combined system of deterministic glucose system model described in (1)–(5) and the lag-1 stochastic model. Specifically, Fig. 8 shows the stochastic model forecasts for the 5th and 95th percentiles of future S_I. These values are substituted into (1), and the system of equations are solved over the forecast interval to generate the spread of future BG based on variability in S_I. The spread of forecasted BG is compared to the measured or interpolated value from retrospective data to determine model forecast performance, and in control situations, the lower bound of the BG forecast range is set to a limit of 4 mmol/L.

IV. DISCUSSION

The lag-1 stochastic model presented in this paper has also been employed on a cohort of adult intensive care patients [46], [47]. The results of Lin *et al.* also show that the model produces

TABLE IV
COMPARISON OF PROBABILITY BOUNDS FOR MODIFICATIONS OF KERNEL DENSITY ESTIMATOR ($\sigma'_x = c\sigma_x$ AND $\sigma'_y = c\sigma_y$)

c	% of S_I within probability bounds		% of BG within prediction bounds	
	[25th - 75th]	[5th - 95th]	[25th - 75th]	[5th - 95th]
0.05	50.8%	90.5%	45.2%	86.2%
0.08	50.8%	90.6%	45.9%	87.1%
0.1	50.7%	90.9%	46.2%	87.5%
0.2	51.7%	90.8%	46.8%	88.3%
0.3	52.2%	90.6%	48.0%	88.8%
0.5	54.7%	90.9%	50.8%	89.5%
1.0	62.6%	93.4%	59.1%	92.2%
2.0	75.4%	96.9%	72.5%	96.4%
Ideal	50%	90%	50%	90%

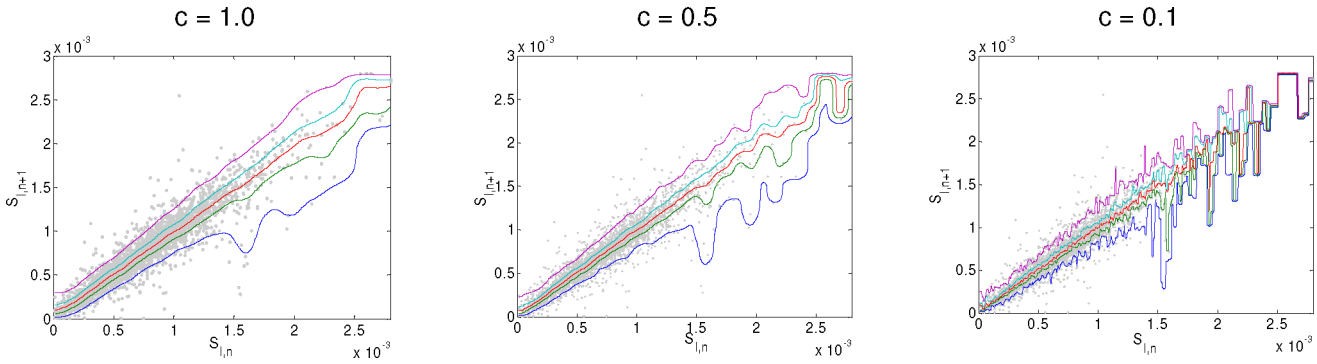

Fig. 6. Probability-bound determination using local variance estimator modified by a constant c. The lower values of c produce a less smooth probability distribution with greater variance at higher S_I. The individual points represent raw S_I data. The solid lines represent the 5%, 25%, 50%, 75%, and 95% probability bounds.

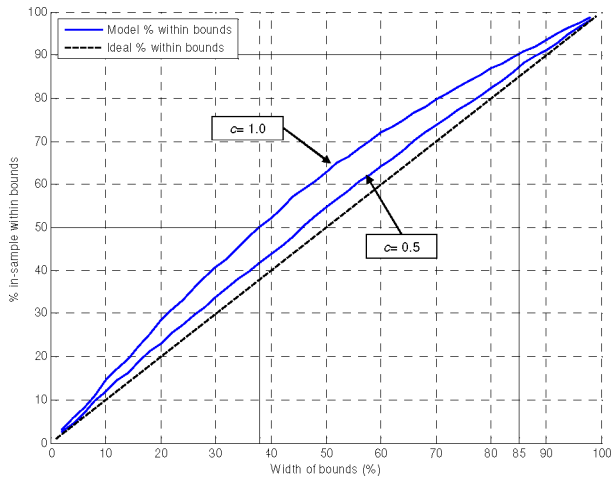

Fig. 7. Comparison of in-sample predicted S_I within arbitrary probability bounds ($2a$) against ideal proportion of predictions within bounds (45° line) for $c = 1.0$ and $c = 0.5$, where interquartile range is the $2a = 50\%$ case.

conservative probability bounds. However, their result of 54.0% within the (25th–75th) percentile bound is far closer to the ideal 50%. Hence, there appear to be unique and significant differences in the variation of model-based S_I between adults and neonates. Additionally, the model-based S_I parameter used in this study is also model-specific, and thus, may also account for different physiological effects in neonates compared to adults.

The kernel density estimator method employed in this stochastic model produces a smooth, physiologically likely distribution, and a conservative model. This conservatism can provide a layer of safety as wider probability bounds would be more likely to capture dynamics and changes not observed in the cohort used to fit the model. However, wider coverage bands may also impact on glycemic control performance, as using a conservatively wide probability band to avoid potential hypoglycemia may needlessly force a controller to maintain a mildly hyperglycemic state. The overall BG width of the (5th–95th) percentile probability band for $c = 1.0$ was 2.32 mmol/L, which would likely have a significant impact on performance for a controller targeting a typical 4–7 mmol/L target range.

A tradeoff between model bias and variance is thus required. The cross validation showed consistent results, suggesting that the cohort dataset is large enough to satisfy the assumption that the model contains enough data points to reasonably reflect the vast majority of target patients presented in the Christchurch Women's Hospital NICU. Modifying the local data density variance estimator showed that less variance ($c < 1.0$) resulted in distributions that more accurately reflected the observed data prediction coverage. The ideal value of the adjustment parameter c was found to be in the range of 0.1–0.5. However, Fig. 6 shows that the probability bounds of the distribution for relatively small c are not smooth, suggesting that this particular distribution is overmodeling the data, where a smoother variation is physiologically more likely. The method shown in Fig. 7

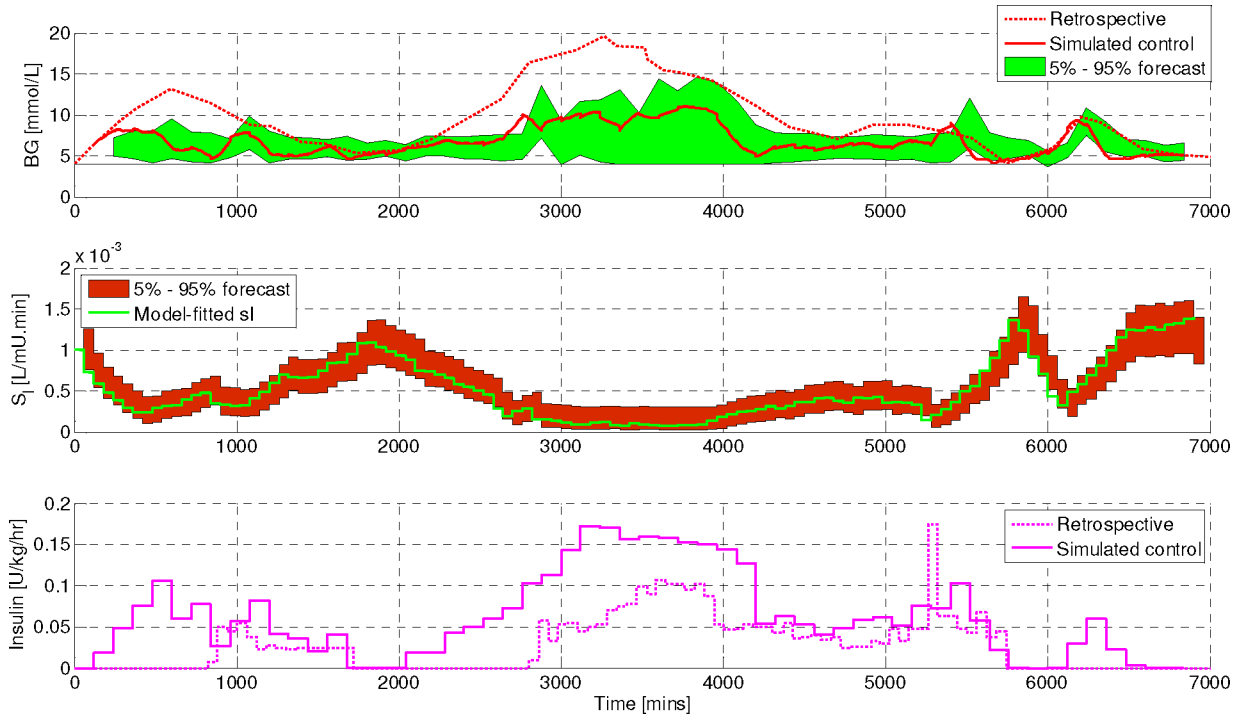

Fig. 8. Simulated trial using model-based control with stochastic model forecasts. The top panel shows blood glucose concentration under simulated control (solid line) compared to retrospective control (dashed line). The middle panel shows model-fitted S_I. The bottom panel shows administration of insulin during simulated control (solid line) compared to retrospective data (dashed line). The shaded areas in the top and middle panels show the 5th–95th percentile of forecasted BG and S_I.

provides a means to produce smooth probability bounds with a customizable tradeoff between glycaemic control performance and hypoglycemic protection. Overall, $c = 0.5$ appeared to provide the most suitable tradeoff between model bias and variance for this cohort.

The results in Fig. 5 suggest that the overestimation of the probability bounds does not occur in regions of sparse data, but rather in regions of dense data. The extension of the model to incorporate lag-2 effects in (10)–(12) had a minimal effect on this dataset. Thus, the local data density variance estimator may be a source of the overestimation. The variance estimator employed here is aligned with the cardinal axes—the major and minor axis of the ellipse that forms from the contours of each individual distribution in (8) is aligned in the x and y directions. A further modification may incorporate a rotation of the distribution-–such that the variance in each distribution is described by three parameters (σ_x, σ_y, and θ) [54] to represent scaling in the x and y directions and rotation, respectively.

Clinically, the absence of lag-2 effects is interesting. It says that variation is hour-to-hour in these neonates and effectively random over that period with no buildup. A second clinical outcome or interpretation is that major changes in the neonate's condition are not likely over a longer period and are, thus, more acute. The lack of significant lag-2 effects appears to indicate that significant changes in S_I, and thus, infant condition may occur largely within 1-h windows. A detailed prospective study, possibly utilizing continuous glucose monitoring, may provide more data to further clarify this preliminary result.

The cohort data represents 3567 h of fitted S_I data over 25 patients. BG measurement density for these patients was typically 2–4 per hour. Thus, there may be some effect introduced by interpolating between BG measurements to fit S_I. However, a lag-1 model produced by only taking values of the S_I parameter one hour before and one hour after each BG measurement still yielded 64.0% of predicted S_I within the 25th–75th percentiles, overshooting the 50% expected value. This result suggests that the BG interpolation is not playing a significant role in this dataset. Higher BG measurement density may reveal more dynamics that could be used to refine the BG system model, and subsequently, the stochastic model. However, such greater measurement density is ethically difficult in the very low-blood-volume NICU population [3].

The nonparametric formulation of the kernel density model automatically accounts for multimodality, which may reveal patterns in large changes in S_I. Clinically, such a sudden or large change could be due to a sudden worsening of condition. Thus, the multimodal model may provide some measure of estimating the risk of sudden significant change (for the worse), particularly at higher S_I, which might offer some significant clinical benefit.

Overall, this stochastic method provides predictions based on a cohort-wide dataset. The prediction bounds for less dynamic patients would typically be more conservative than necessary to account for more dynamic patients that make up the patient population. Thus, the probability bounds are optimized in a cohort sense, but not necessarily on a per-patient basis. Statistical methods, such as autoregressive integrated moving average

(ARIMA) modeling, may provide enhanced prediction performance by customizing the model to the individual patient in real time. However, such models require substantial individualized patient data (e.g., 12–48 h) that may not be available at the commencement of real-time glycaemic control for a given infant. Real-time continuous glucose monitors have been used in neonatal cohorts [55] and may provide additional data for more accurate parameter fitting and forecasting; however, readings on current devices exhibit wide confidence bands, and lower sensitivity and specificity at low BG [55]. Thus, the cohort-wide model presented here could be employed to provide prediction bounds until a suitable amount of data are generated to employ a reliable patient-specific model. Semi-Markov methods may also be employed in S_I forecasting, and can provide an avenue to assess the effect of variable BG measurement and control intervention timings to test robustness to real-world uncertainties and delays.

V. Conclusion

Lag-1 and lag-2 stochastic models are developed to provide S_I predictions based on a set of identified, time-varying S_I data for a neonatal intensive care cohort. The model provides prediction estimators with greater, more conservative, coverage than expected from the probability bounds. Incorporating lag-2 effects did not improve the coverage proportion, and greater coverage overestimation in regions of higher data density pointed to the variance estimator based on local data density as a likely source of overestimation. Modifying the data density estimator by introducing a constant scaling factor showed that appropriate coverage was obtained at approximately 10%–50% of the original value. However, the probability bounds were no longer smooth or as physiologically realistic for very low values near 10%. A value of $c = 0.5$ provided the best tradeoff of bias and variance. Smooth probability bounds containing an appropriate proportion of prediction coverage can be obtained by choosing probability bounds to obtain the desired prediction and glycaemic control performance.

Finally, the model and approach has also provided useful clinical insight. The model skew in distribution at higher $S_{I,n}$ values to account for sudden, larger negative changes in S_I that appears to match clinical reality and provides insight, for at least this cohort, into the risk or likelihood of such changes.

References

[1] A. Le Compte, "Modelling the glucose–insulin regulatory system for glycaemic control in neonatal intensive care," in *Mechanical Engineering*. Christchurch, New Zealand: Univ. Canterbury, 2009.

[2] C. E. Hann, J. G. Chase, J. Lin, T. Lotz, C. V. Doran, and G. M. Shaw, "Integral-based parameter identification for long-term dynamic verification of a glucose-insulin system model," *Comput. Methods Progr. Biomed.*, vol. 77, pp. 259–270, 2005.

[3] R. M. Cowett and H. M. Farrag, "Selected principles of perinatal–neonatal glucose metabolism," *Semin. Neonatol.*, vol. 9, pp. 37–47, 2004.

[4] H. S. Dweck and G. Cassady, "Glucose intolerance in infants of very low birth weight," *Pediatrics*, vol. 53, pp. 189–195, 1974.

[5] R. M. Cowett, W. Oh, A. Pollak, R. Schwartz, and B. S. Stonestreet, "Glucose disposal of low birth weight infants: Steady state hyperglycemia produced by constant intravenous glucose infusion," *Pediatrics*, vol. 63, pp. 389–396, 1979.

[6] G. R. Ditzenberger, S. D. Collins, and N. Binder, "Continuous insulin intravenous infusion therapy for VLBW infants," *J. Perinatal Neonatal Nurs.*, vol. 13, pp. 70–82, 1999.

[7] M. S. Agus, P. J. Javid, D. P. Ryan, and T. Jaksic, "Intravenous insulin decreases protein breakdown in infants on extracorporeal membrane oxygenation," *J. Pediatr. Surg.*, vol. 39, pp. 839–844, 2004.

[8] M. S. Agus, P. J. Javid, H. G. Piper, D. Wypij, C. P. Duggan, D. P. Ryan, and T. M. Jaksic, "The effect of insulin infusion upon protein metabolism in neonates on extracorporeal life support," in *Proc. 126th Annu. Meeting Amer. Surg. Assoc. Ann. Surg. Sci. Papers*, 2006, vol. 244, pp. 536–544.

[9] H. M. Farrag, L. M. Nawrath, J. E. Healey, E. J. Dorcus, R. E. Rapoza, W. Oh, and R. M. Cowett, "Persistent glucose production and greater peripheral sensitivity to insulin in the neonate vs. the adult," *Amer. J. Physiol.*, vol. 272, pp. E86–E93, 1997.

[10] B. B. Poindexter, C. A. Karn, and S. C. Denne, "Exogenous insulin reduces proteolysis and protein synthesis in extremely low birth weight infants," *J. Pediatr.*, vol. 132, pp. 948–953, 1998.

[11] F. Thabet, J. Bourgeois, B. Guy, and G. Putet, "Continuous insulin infusion in hyperglycaemic very-low-birth-weight infants receiving parenteral nutrition," *Clin. Nutr.*, vol. 22, pp. 545–547, 2003.

[12] A. H. Hemachandra and R. M. Cowett, "Neonatal hyperglycemia," *Pediatr. Rev.*, vol. 20, pp. 16e–24e, 1999.

[13] H. M. Farrag and R. M. Cowett, "Glucose homeostasis in the micropremie," *Clin. Perinatol.*, vol. 27, pp. 1–22, 2000.

[14] W. J. Powers, J. L. Rosenbaum, C. S. Dence, J. Markham, and T. O. Videen, "Cerebral glucose transport and metabolism in preterm human infants," *J. Cereb. Blood Flow Metab.*, vol. 18, pp. 632–638, 1998.

[15] K. C. Ho, U. Roessmann, L. Hause, and G. Monroe, "Newborn brain weight in relation to maturity, sex, and race," *Ann. Neurol.*, vol. 10, pp. 243–246, 1981.

[16] R. M. Cowett, W. Oh, and R. Schwartz, "Persistent glucose production during glucose infusion in the neonate," *J. Clin. Invest.*, vol. 71, pp. 467–475, 1983.

[17] D. I. Alaedeen, M. C. Walsh, and W. J. Chwals, "Total parenteral nutrition-associated hyperglycemia correlates with prolonged mechanical ventilation and hospital stay in septic infants," *J. Pediatr. Surg.*, vol. 41, pp. 239–244, 2006.

[18] M. Raney, A. Donze, and J. R. Smith, "Insulin infusion for the treatment of hyperglycemia in low birth weight infants: examining the evidence," *Neonatal Netw.*, vol. 27, pp. 127–140, 2008.

[19] G. Cassady, "Plasma volume studies in low birth weight infants," *Pediatrics*, vol. 38, pp. 1020–1027, 1966.

[20] J. A. Leipala, M. Talme, J. Viitala, U. Turpeinen, and V. Fellman, "Blood volume assessment with hemoglobin subtype analysis in preterm infants," *Biol. Neonate*, vol. 84, pp. 41–44, 2003.

[21] D. Mitanchez-Mokhtari, N. Lahlou, F. Kieffer, J.-F. Magny, M. Roger, and M. Voyer, "Both relative insulin resistance and defective islet {beta}-cell processing of proinsulin are responsible for transient hyperglycemia in extremely preterm infants," *Pediatrics*, vol. 113, pp. 537–541, 2004.

[22] J. Simpson and T. Stephenson, "Regulation of extracellular fluid volume in neonates," *Early Hum. Dev.*, vol. 34, pp. 179–190, 1993.

[23] J. M. Lorenz, L. I. Kleinman, G. Ahmed, and K. Markarian, "Phases of fluid and electrolyte homeostasis in the extremely low birth weight infant," *Pediatrics*, vol. 96, pp. 484–489, 1995.

[24] G. Hartnoll, P. Betremieux, and N. Modi, "Body water content of extremely preterm infants at birth," *Arch. Dis. Childhood*, vol. 83, pp. F56–F59, 2000.

[25] K. S. Bidiwala, J. M. Lorenz, and L. I. Kleinman, "Renal function correlates of postnatal diuresis in preterm infants," *Pediatrics*, vol. 82, pp. 50–58, 1988.

[26] D. E. Hertz, C. A. Karn, Y. M. Liu, E. A. Liechty, and S. C. Denne, "Intravenous glucose suppresses glucose production but not proteolysis in extremely premature newborns," *J. Clin. Invest.*, vol. 92, pp. 1752–1758, 1993.

[27] S. P. Hays, B. Smith, and A. L. Sunehag, "Hyperglycemia is a risk factor for early death and morbidity in extremely low birth-weight infants," *Pediatrics*, vol. 118, pp. 1811–1818, 2006.

[28] L. S. Kao, B. H. Morris, K. P. Lally, C. D. Stewart, V. Huseby, and K. A. Kennedy, "Hyperglycemia and morbidity and mortality in extremely low birth weight infants," *J. Perinatol.*, vol. 26, pp. 730–736, 2006.

[29] N. J. Hall, M. Peters, S. Eaton, and A. Pierro, "Hyperglycemia is associated with increased morbidity and mortality rates in neonates with necrotizing enterocolitis," *J. Pediatr. Surg.*, vol. 39, pp. 898–901, 2004.

[30] S. C. Kalhan, A. Oliven, K. C. King, and C. Lucero, "Role of glucose in the regulation of endogenous glucose production in the human newborn," *Pediatr. Res.*, vol. 20, pp. 49–52, 1986.
[31] A. Sunehag, M. Haymond, R. Schanler, P. Reeds, and D. Bier, "Gluconeogenesis in very low birth weight infants receiving total parenteral nutrition," *Diabetes*, vol. 48, pp. 791–800, 1999.
[32] E. E. Tyrala, X. Chen, and G. Boden, "Glucose metabolism in the infant weighing less than 1100 grams," *J. Pediatr.*, vol. 125, pp. 283–287, 1994.
[33] Kempen, A. A. Van, J. A. Romijn, A. F. Ruiter, M. T. Ackermans, E. Endert, J. H. Hoekstra, J. H. Kok, and H. P. Sauerwein, "Adaptation of glucose production and gluconeogenesis to diminishing glucose infusion in preterm infants at varying gestational ages," *Pediatr. Res.*, vol. 53, pp. 628–634, 2003.
[34] J. W. Collins, Jr., M. Hoppe, K. Brown, D. V. Edidin, J. Padbury, and E. S. Ogata, "A controlled trial of insulin infusion and parenteral nutrition in extremely low birth weight infants with glucose intolerance," *J. Pediatr.*, vol. 118, pp. 921–927, 1991.
[35] Y. E. Vaucher, P. D. Walson, and G. Morrow, 3rd, "Continuous insulin infusion in hyperglycemic, very low birth weight infants," *J. Pediatr. Gastroenterol. Nutr.*, vol. 1, pp. 211–217, 1982.
[36] N. D. Binder, P. K. Raschko, G. I. Benda, and J. W. Reynolds, "Insulin infusion with parenteral nutrition in extremely low birth weight infants with hyperglycemia," *J. Pediatr.*, vol. 114, pp. 273–280, 1989.
[37] S. M. Ng, J. E. May, and A. J. Emmerson, "Continuous insulin infusion in hyperglycaemic extremely-low-birth-weight neonates," *Biol. Neonate*, vol. 87, pp. 269–272, 2005.
[38] S. Ostertag, L. Jovanovic, B. Lewis, and P. Auld, "Insulin pump therapy in the very low birth weight infant," *Pediatrics*, vol. 78, pp. 625–630, 1986.
[39] K. S. Kanarek, M. L. Santeiro, and J. I. Malone, "Continuous infusion of insulin in hyperglycemic low-birth weight infants receiving parenteral nutrition with and without lipid emulsion," *J. Parenter. Enteral Nutr.*, vol. 15, pp. 417–420, 1991.
[40] P. Mena, A. Llanos, and R. Uauy, "Insulin homeostasis in the extremely low birth weight infant," *Semin. Perinatol.*, vol. 25, pp. 436–446, 2001.
[41] V. Kairamkonda, "Does continuous insulin infusion improve glycaemic control and nutrition in hyperglycaemic very low birth weight infants?," *Arch. Dis. Child.*, vol. 91, pp. 76–79, 2006.
[42] J. Chase, G. M. Shaw, X. W. Wong, T. Lotz, J. Lin, and C. E. Hann, "Model-based glycaemic control in critical care—A review of the state of the possible," *Biomed. Signal Process. Control*, vol. 1, pp. 3–21, 2006.
[43] J. G. Chase, G. M. Shaw, T. Lotz, A. LeCompte, J. Wong, J. Lin, T. Lonergan, M. Willacy, and C. E. Hann, "Model-based insulin and nutrition administration for tight glycaemic control in critical care," *Curr. Drug Deliv.*, vol. 4, pp. 283–296, 2007.
[44] K. C. McCowen, A. Malhotra, and B. R. Bistrian, "Stress-induced hyperglycemia," *Crit. Care Clin.*, vol. 17, pp. 107–124, 2001.
[45] D. P. Barker and N. Rutter, "Stress, severity of illness, and outcome in ventilated preterm infants," *Arch. Dis. Childhood*, vol. 75, pp. F187–E190, 1996.
[46] J. Lin, D. Lee, J. Chase, C. Hann, T. Lotz, and X. Wong, "Stochastic modelling of insulin sensitivity variability in critical care," *Biomed. Signal Process. Control*, vol. 1, pp. 229–242, 2006.
[47] J. Lin, D. Lee, J. G. Chase, G. M. Shaw, A. Le Compte, T. Lotz, J. Wong, T. Lonergan, and C. E. Hann, "Stochastic modelling of insulin sensitivity and adaptive glycemic control for critical care," *Comput. Methods Progr. Biomed.*, vol. 89, pp. 141–152, 2008.
[48] R. Hovorka, F. Shojaee-Moradie, P. V. Carroll, L. J. Chassin, I. J. Gowrie, N. C. Jackson, R. S. Tudor, A. M. Umpleby, and R. H. Jones, "Partitioning glucose distribution/transport, disposal, and endogenous production during IVGTT," *Amer. J. Physiol. Endocrinol. Metab.*, vol. 282, pp. E992–E1007, 2002.
[49] X. W. Wong, J. G. Chase, G. M. Shaw, C. E. Hann, T. Lotz, J. Lin, I. Singh-Levett, L. J. Hollingsworth, O. S. Wong, and S. Andreassen, "Model predictive glycaemic regulation in critical illness using insulin and nutrition input: A pilot study," *Med. Eng. Phys.*, vol. 28, pp. 665–681, 2006.
[50] A. Le Compte, J. Chase, A. Lynn, C. Hann, G. Shaw, X. Wong, and J. Lin, "Blood glucose controller for neonatal intensive care: Virtual trials development and 1st clinical trials," *J. Diab. Sci. Technol.*, vol. 3, pp. 1066–1081, 2009.
[51] H. M. Farrag, E. J. Dorcus, and R. M. Cowett, "Maturation of the glucose utilization response to insulin occurs before that of glucose production in the preterm neonate," *Pediatr. Res.*, vol. 39, p. 308, 1996.
[52] A. Le Compte, A. Lynn, J. Chase, G. Shaw, G. Russell, A. Blakemore, D. Lee, X. Wong, J. Lin, and C. E. Hann, "Neonatal glycaemic control—Model validation and in silico virtual patient trials," presented at the 8th Annu. Diab. Technol. Meeting, Bethesda, MD, 2008.
[53] A. W. Bowman and A. Azzalini, *Applied Smoothing Techniques for Data Analysis: The Kernel Approach With S-Plus Illustrations*. New York: Clarendon, 1997.
[54] J. W. Kern, T. L. McDonald, S. C. Amstrup, G. M. Durner, and W. P. Erickson, "Using the bootstrap and fast Fourier transform to estimate confidence intervals of 2D kernel densities," *Environ. Ecol. Statist.*, vol. 10, pp. 405–418, 2003.
[55] K. Beardsall, A. L. Ogilvy-Stuart, J. Ahluwalia, M. Thompson, and D. B. Dunger, "The continuous glucose monitoring sensor in neonatal intensive care," *Arch. Dis. Child Fetal Neonatal Educ.*, vol. 90, pp. F307–F310, 2005.

Authors' photographs and biographies not available at the time of publication.